ELSEVIER

Journal of Hazardous Materials 43 (1995) 195–216

JOURNAL OF HAZARDOUS MATERIALS

Solid particle penetration into enclosures

S. Lewis[1]

Israel Atomic Energy Commission, Soreq Nuclear Research Center, Yavne 81800, Israel

Received 26 July 1994; accepted in revised form 21 March 1995

Abstract

Protection factors against toxic vapors for enclosures such as vehicles and shelters are commonly evaluated on the basis of the behavior of a simulant vapor. Mechanisms influencing protection against solid particles have yet to be integrated into integrity-testing procedures. The scarcity of empirical studies which could provide the basis for such procedures suggested a program whose objectives would be to provide means for measuring size-dependent solid particle protection factors for various exposure scenarios and for expressing the relevant mechanisms in model calculations. These could then aid in the design of such procedures.

A system providing a flexible infrastructure for experimenting with controlled challenge scenarios was assembled outdoors in an open-ended agricultural cloche. A sealed enclosure located at the end of the cloche far from the dissemination apparatus enabled testing of solid particle challenge penetration through well-defined apertures under controlled ventilation dynamics. A computer model was written to calculate protection factors for vapor and solid particles using both theoretical models and empirical data. The experimental system provided data for the calibration and verification of the model.

Keywords: Solid particles; Protection factors; Penetration

1. Introduction

The vapor protection factor, PF_V, for an enclosure is defined as the ratio of the dose (concentration-time integral) which would result from exposure to an outside concentration, C_o, during cloud passage time, T, to that dose accumulated inside up to some time $t \geqslant T$. The governing parameter is volumetric air exchange, or infiltration rate, R. This determines the rates both of vapor penetration and its flushing out after the cloud has passed. For a uniform vapor exposure and ideal

[1] Work performed while on sabbatical leave at US Army Edgewood Research and Engineering Center, Aberdeen Proving Ground, MD, USA.

SSDI 0304-3894(95)00037-2

mixing in an enclosure, the balance equation for a single well-mixed compartment leads to (see Appendix):

$$PF_V = \frac{R \cdot T}{R \cdot T + \exp(-R \cdot t) \cdot (1 - \exp(R \cdot T))}. \quad (1)$$

Given the air exchange rate, perhaps measured with a tracer gas such as SF_6, the protection factor for an ideal, non-condensing vapor may readily be estimated.

This widely accepted definition allows neither filtering of penetrating molecules by the residual cracks nor surface losses within the enclosure. Both of these mechanisms would clearly augment respiratory protection against particulate or condensing contaminants, while subsequent resuspension or evaporation of condensed volatile contaminants would re-contribute to the internal dose.

2. Solid particle protection factor theoretical model

A literature search of sheltering against particulate matter revealed few comprehensive treatments of the problem. For example, works reported by Roed [1], Brenk and De Witt [2] and Engelmann [3, 4] concerning sheltering effectiveness of buildings and vehicles define a transfer factor or dose reduction factor, the inverse of the protection factor, in terms of particulate removal phenomena. In the above-mentioned references underlying size-dependent mechanisms were not investigated. In the following paragraphs, works published which deal with these mechanisms separately are discussed. These were subsequently adopted for integration into a computer model calculating the size-dependent particulate protection factor for an enclosure.

Crack filtering and interior surface deposition of particles involve three removal mechanisms: diffusion, gravitational settling and turbulent impaction. If a size-dependent filtering factor, f_p, and settling rate, β_p, are included with the air exchange rate as removal terms in the single compartment balance model, an expression for the particulate protection factor, PF_p, is obtained (see Appendix):

$$PF_p = \frac{R_p \cdot T}{\left(\frac{f_p \cdot R}{R_p}\right)(R_p \cdot T + \exp(-R_p \cdot t) \cdot (1 - \exp(R_p \cdot T)))}, \quad (2)$$

where $R_p = R + \beta_p$ [1/s]. In the experimental program, the exposure system provided measurements relevant to the calculation of the size-dependent protection factors. These were used also to calibrate the theoretical model calculations. Direct measurements of external and internal doses resulting from a particulate cloud challenge yielded the actual protection factors which aided in verifying the model results.

Solid particle settling in enclosures with convective stirring has been widely covered in the literature [5–12] with several efforts at verifying model equations by means of controlled chamber tests. Crump and Seinfeld's [7] equation for particle settling rate

in an enclosure, as shown by Chen et al. [12] for a rectangular chamber, is

$$\beta_p \equiv \frac{2 \cdot U_t}{X_1}\left(\frac{1}{l}+\frac{1}{w}\right)+\frac{U_t}{h}\coth\left(\frac{X_1}{2}\right) \quad [1/s], \tag{3}$$

where l, w and h are the length, width and height, respectively, of the enclosure; U_t is the particle settling velocity, and

$$X_1 = \frac{\pi \cdot U_t}{n_e \sin\left(\frac{\pi}{n_e}\right)(k_e \cdot D_B^{n_e-1})^{1/n_e}}, \tag{4}$$

where k_e and n_e are the coefficient and exponent of the eddy diffusion coefficient given by

$$D_e = k_e \cdot Y^{n_e}, \tag{5}$$

where Y is the distance from the wall and D_B is the Brownian diffusion coefficient. Although a theoretical value of $n_e = 2$ is often accepted, Chen et al. [12] used solid particle settling data to determine both k_e and n_e. The coefficient k_e indicates the intensity of turbulent mixing from all sources such as fans, induced air flow and temperature gradients.

The equation of Crump and Seinfeld [7] was adopted for the protection factor model. As an alternative, the model was designed to accept also experimental settling rate data and to calculate a semi-empirical result.

A review report by Schwendiman and Sutter [13] on the transport of particles through gas leaks discusses the three controlling mechanisms: deposition by molecular diffusion, turbulent impaction and gravitational settling.

Deposition by molecular diffusion is controlled by the diffusion coefficient, aperture length and the air flow rate. Empirical equations, verified for diffusion batteries by Sinclair et al. [14], were adopted for the protection factor model.

Eddy transport of particles to the aperture walls is determined by the inertial properties of the particles in the turbulent field. The fraction lost to turbulent impaction, F_T, is defined by

$$F_T = 1 - \exp\left(-\frac{P \cdot K \cdot l_a}{A \cdot V}\right), \tag{6}$$

where P is the aperture perimeter, A is the cross sectional area, l_a is the length of the aperture path, V is the average velocity and K is the deposition velocity. Lacking experimental values of K, the terminal settling velocity is currently used, resulting in a minimum wall loss.

An approximation for the fraction lost by gravitational settling in a rectangular aperture, stipulating a uniform velocity profile, is given by

$$F_G = \frac{l_a \cdot U_t}{V}. \tag{7}$$

These simplified equations neglect complications such as electrostatic charges, aperture clogging and surface roughness. They are reportedly robust enough to provide useful first-order approximations and have been included in the model to calculate a size-dependent total transport fraction through an aperture as defined by parameter f_p in Eq. (2).

The rate of air exchange in a well-mixed enclosure, R in Eqs. (1) and (2), is estimated by the ratio of the air flowrate to the volume of the enclosure:

$$R \equiv \frac{Q}{V}. \tag{8}$$

A constant differential pressure across a well-defined aperture was chosen as the driving force for particle penetration in the model and in the experimental system. The air flowrate can then be calculated by the crack flow equation:

$$Q = C \cdot A_e \cdot (\mathrm{d}p)^n, \tag{9}$$

where $\mathrm{d}p$ is the differential pressure, n is the characteristic flow exponent which varies between 0.5 and 1.0 depending on the Reynold's number (see [15]), C is a discharge coefficient and A_e is the effective leakage area. The parameters are either estimated or the airflow is measured experimentally.

With the above elements integrated in a computer program solving Eqs. (1) and (2), the particle protection factor can be calculated for given enclosure and aperture dimensions, differential pressure, turbulent mixing regime, challenge duration and particle size spectrum (within a 0.1–10 μm range). The final results are displayed as a matrix of PF_p values across the size spectrum for several differential pressure values. Vapor protection factors are displayed for comparison. If a polydisperse challenge is being studied whose log normal spectral parameters are known or estimated, then the PF_p values are weighted to yield a total protection factor. Figs. 1–4 present sample results for total transport fraction, particle decay rates, particulate protection factors and weighted protection factors for vapor and a chosen polydisperse challenge. The relevant parameters for the run are

- enclosure dimension: $l = 213$ cm, $h = 117$ cm, $w = 167$ cm,
- aperture dimensions: $l = 80$ cm, $h = 0.015$ cm, $w = 4$ cm,
- challenge duration (T): 5 min,
- exposure time (t): 30 min,
- particle desity: 2.7 g/cm^3,
- log normal parameters: geometric mean 1.2, std. dev. 2.284,
- flow exponent (n): 0.5,
- turbulent dissipation: $k_e = 1000$, $n_e = 2.038$,
- differential pressures: -10, -20, and -30 Pa.

The qualitative features of the plots compare well with expected behavior. Total transport fractions through the aperture in Fig. 1 drop sharply at 1 μm diameter. The particle settling rates in Fig. 2 exhibit a minimum value at the confluence of the diffusional and gravitational mechanisms at small and large diameters, respectively. The particulate protection factors in Fig. 3 show strong size-dependence with some

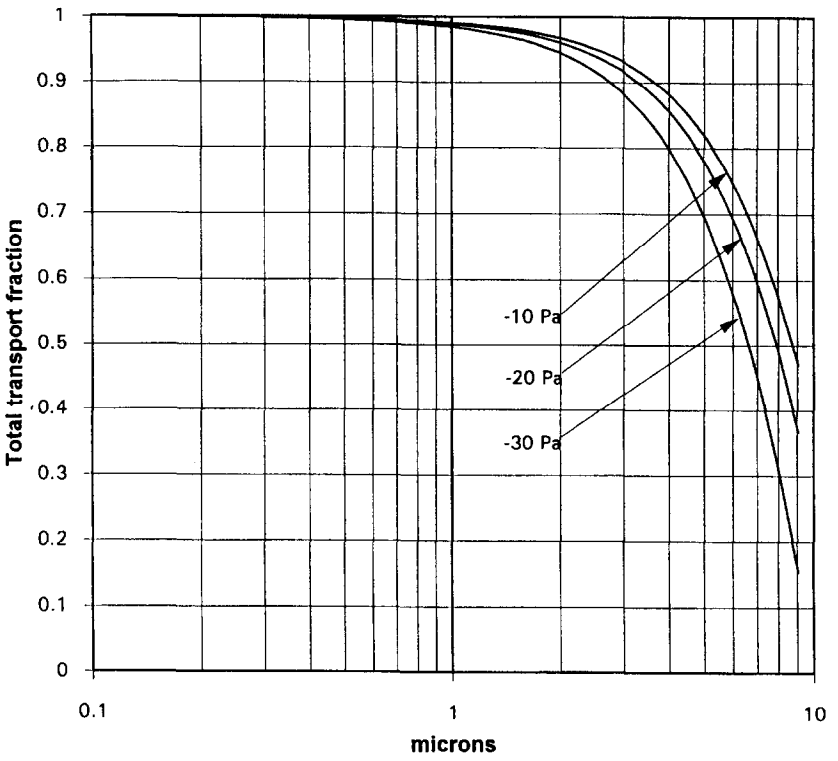

Fig. 1. Modeled total transport fractions as a function of differential pressure.

improvement at the smallest sizes and considerable improvement at the larger sizes. This behavior is a combination of the high diffusional settling rates of the smallest particles and high filtration and gravitational settling rates of the larger particles. The weighted particulate total protection factors in Fig. 4 are correlated with the vapor protection factors through the air exchange rates but exhibit the reduced doses due to particulate removal mechanisms. As the differential pressure increases, the increased air exchange rate reduces the relative advantage obtained by these mechanisms.

3. Experimental system

3.1. Exposure facility

An open-ended agricultural cloche with a semicircular cross-section, anchored on a concrete pad, allows controlled dissemination of solid particles and simulant gases and exposure testing of a sealed enclosure. The 18 m long, 4.3 m wide and 2 m high

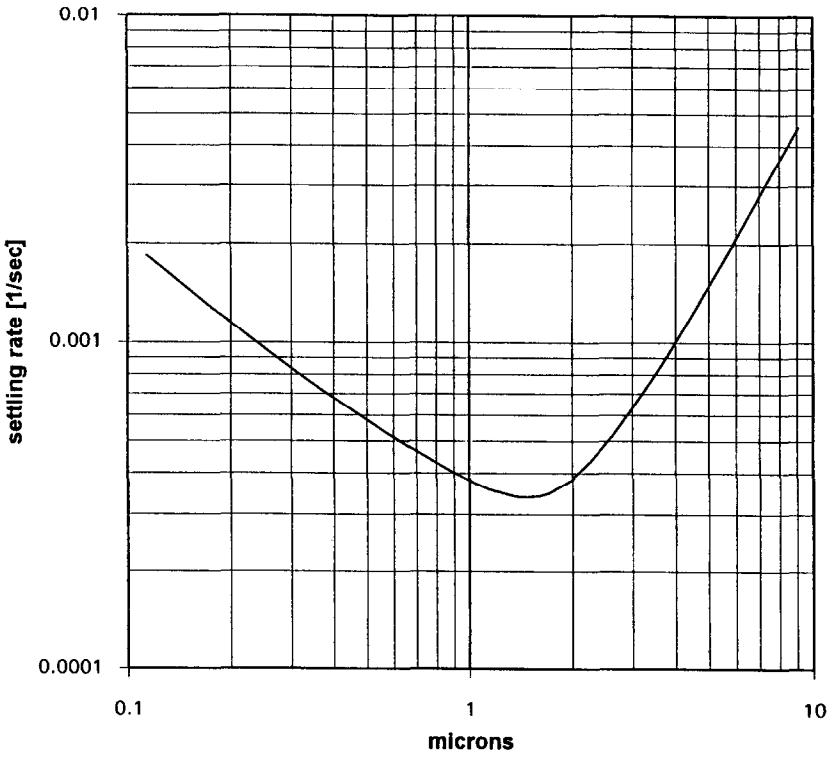

Fig. 2. Modeled solid particle settling rate.

cloche is constructed from semicircular pipes and covered with polyethylene sheeting. Fig. 5 is a schematic diagram of the facility with the dissemination and exposure systems shown at either end.

3.2. Dissemination system

A schematic diagram of the powder dissemination system is shown in Fig. 6. The system is comprised of a Metronics, Inc., Fluorescent Particle Tracer Generator coupled to a pneumatic nozzle. The generator is comprised of a cylindrical powder canister attached to a gear-driven gravity feeder mechanism. The canister is continuously stirred and the gear feeder is simultaneously wiped to maintain free powder flow. The blower attached to the underside of the feeder was removed so that the pneumatic nozzle's powder input tube could instead be connected to the feeder through a plastic funnel. The nozzle is fed by an air compressor operated at 500 kPa. About 5 kPa suction develops at the powder input so that as each parcel of powder drops from a gear tooth into the funnel it is drawn into the nozzle, disaggregated and disseminated. The air flow ratio between nozzle output and powder input is

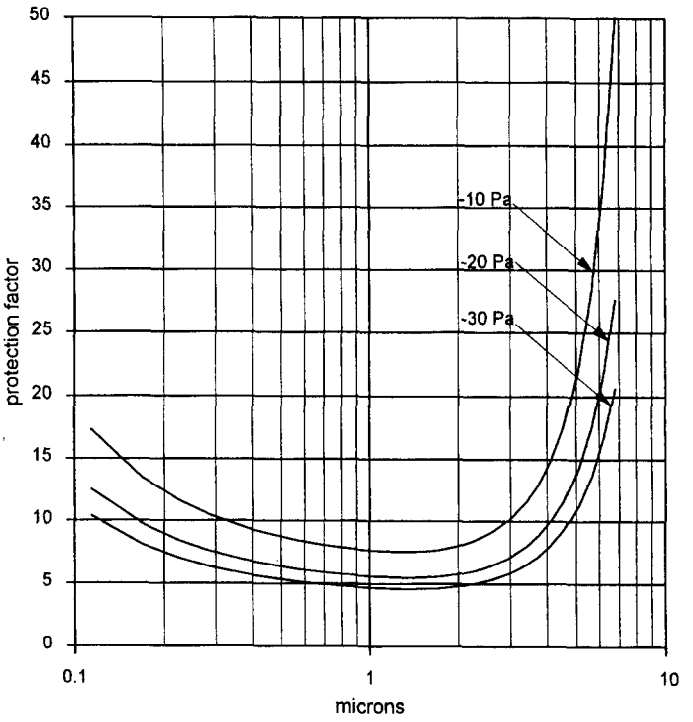

Fig. 3. Modeled solid particle protection factors as a function of differential pressure.

about 50:1, so the disaggregation mechanism at the nozzle outlet is considerably energetic.

The pneumatic nozzle is situated 1.25 m above the ground near one end of the cloche. Behind it are three 24″ shop fans in a row facing down the length of the cloche. A table fan placed close to the nozzle and facing back into the stream of disseminating particles spreads the stream across the plane of the larger fans and facilitates uniform crosswise mixing. This simple system generates a 1–1.5 m/s breeze at the far end of the cloche and powder mass concentrations with a spread of only 10–20% across the cloche area. Challenge concentrations up to several tens of mg/m^3 can be produced, depending on powder composition, feed rate, and fan power.

When vapor penetration is to be measured, SF_6 tracer gas is disseminated through a rotameter from a point near the nozzle so that the vapor stream benefits from the same mechanical dispersion as does the powder stream.

3.3. Exposure testing enclosure

The exposure testing enclosure is a fiberglass gas mask testing chamber having several Plexiglas windows and one large door. The airlock wall was left out to make

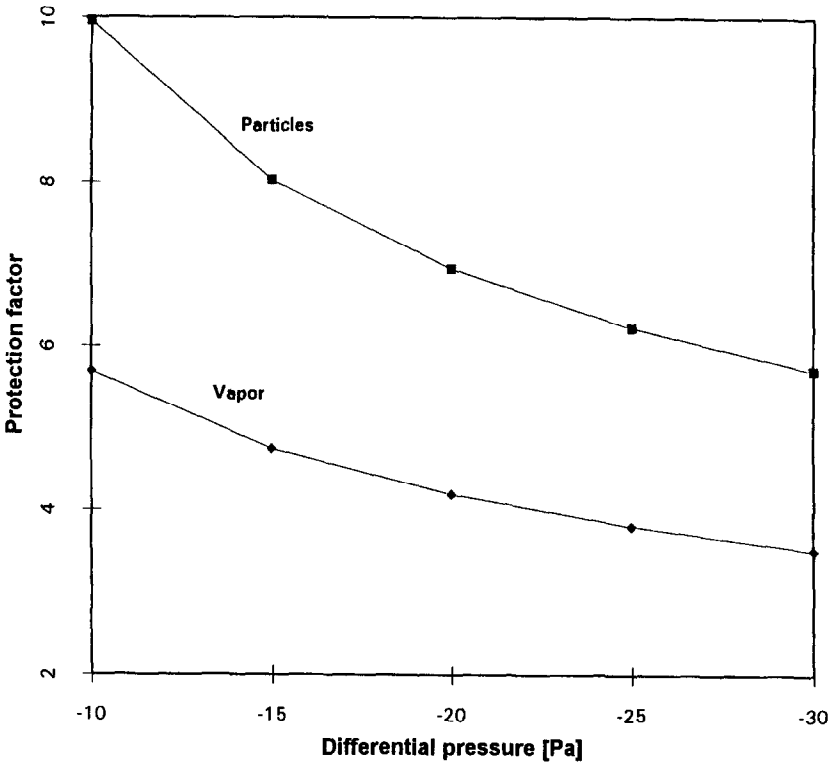

Fig. 4. Log normal-weighted solid particle and vapor protection factors as a function of differential pressure.

a single 4.43 m^3 volume. The chamber lies on its side on a small carriage for ease in movement. All the chamber joints were reconstructed with 6 mm thick rubber stripping to ensure air tightness. Bulkheads were provided for signal cables and air sampling tubes. A centrifugal blower at the opposite end of the cloche is connected to the chamber through 9 cm diameter plastic tubing to provide constant differential pressure, measured between the chamber and the environment by an Endevco Model 8510B piezoresistive pressure transducer. A Kurz Model 505 mass flow meter measures air flowrate.

One window of the chamber, facing toward the dissemination apparatus, was replaced by two 10 mm thick plates of perspex pressed onto a thick rubber seal by quick-release clamps bolted to the wall. The 85 cm long plates are separated by feeler gauges to provide a well-defined aperture in the chamber wall. Additional perspex strips may be added at the interface as desired to provide aperture thicknesses up to 50 mm.

The chamber is instrumented to measure inside and outside particle and vapor concentrations, temperature differences and relative humidity. Three MIE, Inc. RAS-2

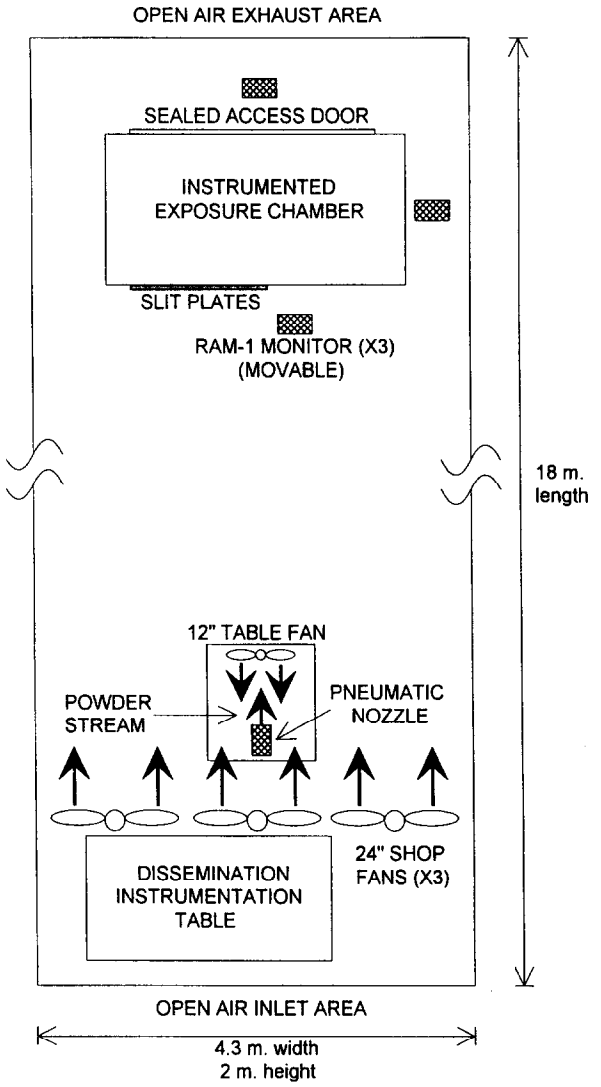

Fig. 5. Schematic diagram of the exposure facility

Real-time Particle Sensors situated around the chamber obtain challenge mass concentration data in the range 0.01–100 mg/m^3 with a 0.2 s response time. The sensors were calibrated against several test powders with various size spectra and compositions and found to produce acceptably similar readings. Inside the chamber an MIE, Inc. RAM-1 Real-time Particle Monitor measures penetrating particle mass concentration in the range 0.001–200 mg/m^3 with response time down to 0.5 s.

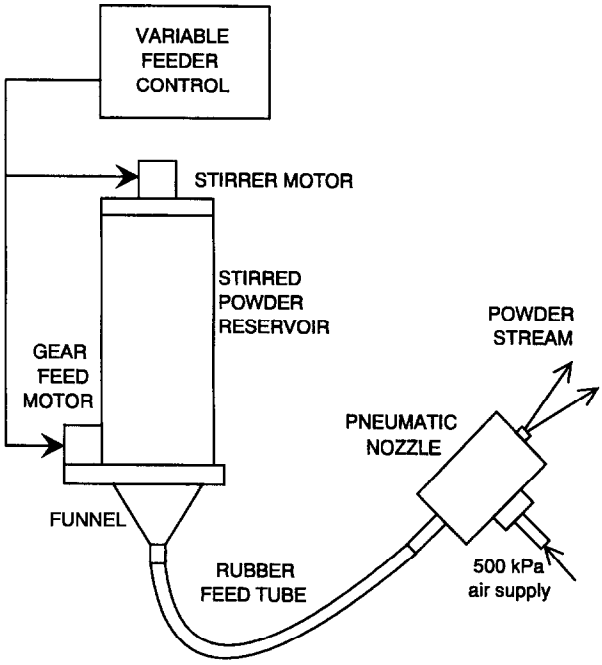

Fig. 6. Schematic diagram of the dissemination system.

A PMS LAS-X Laser Particle Spectrometer inside the chamber measures particle size spectra. 64 bins are provided in the size range 0.12–7.5 μm. When needed, the LAS-X is linked to a TSI Model 3302 Diluter to provide lower countrates. Since the spectrometer has a cooling fan and sample air vent to the outside, the 'quiescent' mixing condition mentioned later includes, by necessity, this minimum of mechanical energy. The LAS-X can sample from outside the chamber through a dedicated bulkhead opening when the particulate challenge is to be characterized. Data output is sent by RS-232 to a portable computer for analysis.

A Foxboro, Inc. MIRAN-1A Infrared Gas Analyzer monitors SF_6 tracer gas challenge concentration while a portable electron capture gas chromatograph with an automatic sampling manifold measures vapor penetration into the enclosure.

4. Experimental results

4.1. Disseminated particle size spectra

Only powders acceptable by environmental safety standards have been used as candidate simulants. Those employed to date include

- Asbestos-free talc,
- Hydrophobic Aerosils (DeGussa fumed silica),
- Hydrophobic Sipernats (DeGussa precipitated silica),
- Aluminum oxide,
- Titanium dioxide (various manufacturers),
- Arizona road dust (0–5 μm nominal).

Of first concern was the efficiency of the powder feeder and pneumatic nozzle in disagglomerating and disseminating candidate simulant powders. Several powders have been tested for flowability in the feeder and for the size spectra obtained after dissemination. Fig. 7 shows aerodynamic diameter spectra collected following dissemination and transport over a distance of 15 m. The aerosils and sipernats, although disseminated as agglomerates of varying sizes, have primary particle sizes in the 15–20 nm range, which cannot be distinguished by the LAS-X spectrometer. The disseminated spectra of some agglomerated, polydisperse powders can be tailored to some extent by changing the pneumatic nozzle energy or by returning the original blower to the feeder in place of the nozzle.

4.2. Particle settling rate measurements

The considerable divergence between theory and measurements of solid particle settling rates noted in the cited literature and the difficulty in determining turbulent energy dissipation parameters for stirred settling prompted a series of settling rate measurements in the chamber. Tests were carried out by exposing the chamber interior to a continuous cloud of disseminated powder and then immediately sealing the door. The mass concentration was monitored to ensure uniform mixing and minimum agglomeration before spectra were collected by the LAS-X every four minutes. A variety of turbulence scenarios were obtained by operating muffin fans inside the chamber.

Data were analyzed by a log-linear optimization of particle counts in individual size bins vs. time to yield best values of the settling rates:

$$dC(r, t)/dt = -\beta_p C(r, t). \tag{10}$$

In all cases the settling rates fit the exponential function with a correlation coefficient better than 0.9. Shown in Fig. 8 are results for talc, which spectrum provides a convenient tool for simultaneous, polydisperse measurements. Increasing the turbulent mixing intensity between runs results in the settling rate curves uniformly shifting to higher values. Additional measurements with other powders having narrower size spectra yielded consistent results.

These data are useful in estimating empirical values for the eddy dissipation parameters in Eq. (5). However, attempts at fitting the model Eq. (3) to the experimental data have not been satisfactory as, for all powders tried to date, settling rates of particles above about 1 μm diameter in this enclosure are far lower than predicted by the Crump and Seinfeld model. Unambiguous parameter values have not been obtained although the model equations did reproduce identical results when tested with published data (for example, Van de Vate's [5] data with the best-fitted values

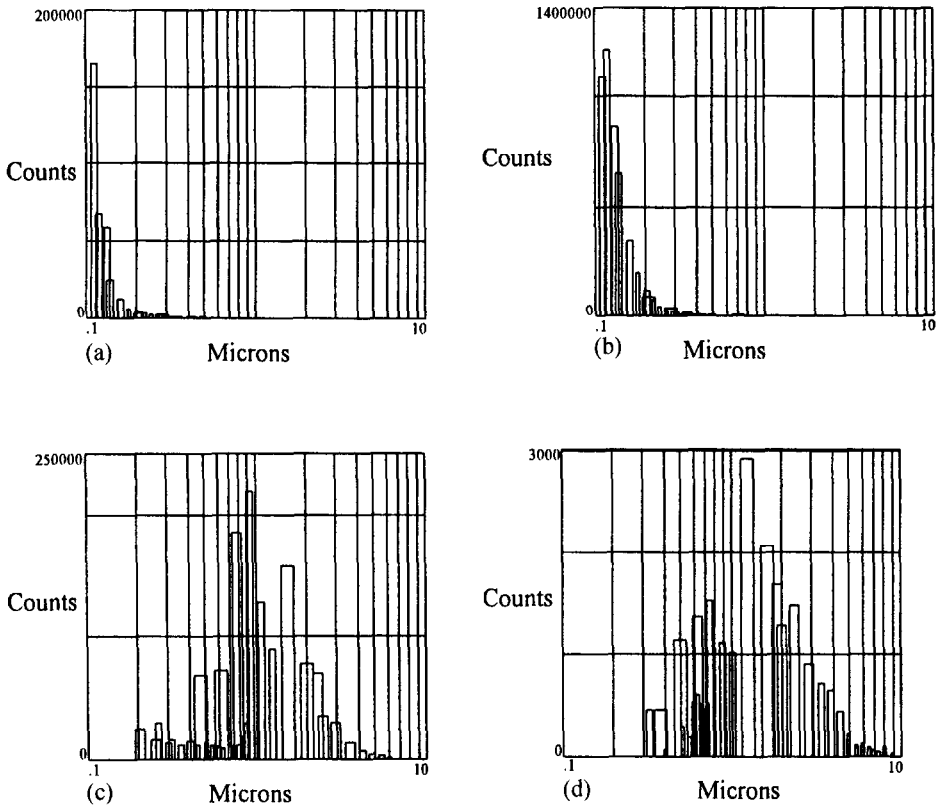

Fig. 7. Pneumatic nozzle disseminated particle spectra: (a) Aerosil 976 (De Gussa fumed silica). (b) Sipernat D-11 (De Gussa precipitated silica); (c) Titanium dioxide (Tiona RCL-2); and (d) Asbestos-free talc.

given by Chen [12]). Hence, empirical data have been included in the protection factor model for use in verifying measured protection factors.

4.3. Solid particle penetration tests

Several tests were carried out with the objective of investigating the penetration into the chamber of particles in the range 0.1–10 μm. A differential pressure was applied across the aperture which would ensure a significant difference between the protection factors for vapor and solid particles. In one series the same ventilation kinetics and exposure parameters were maintained while different powders were disseminated. A pressure differential of −10 Pa was maintained across a 0.1 mm high slit with 40 mm depth. A challenge passage time of about 0.5 min was produced in each case.

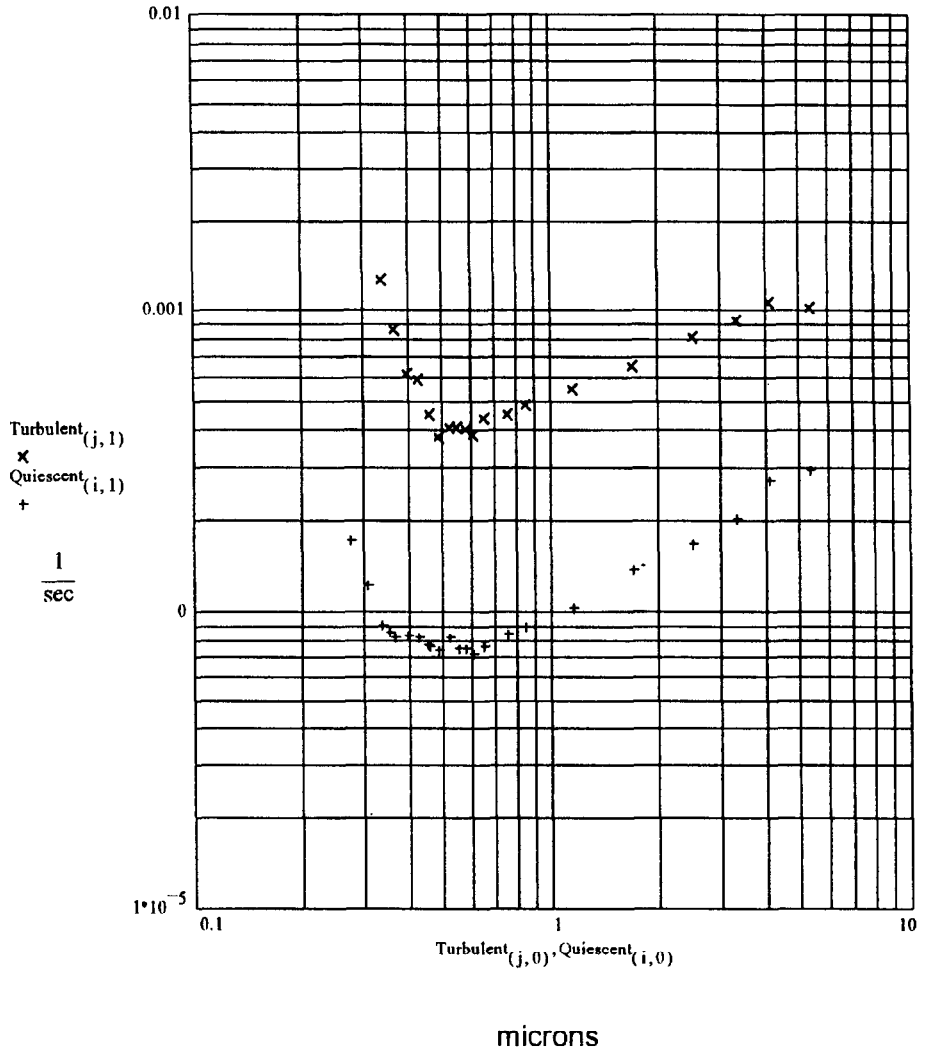

Fig. 8. Experimental settling rates for talc: (×) two muffin fans operating in the enclosure (turbulent); (+) no fans operating (quiescent).

The empirical protection factors, defined as the outside/inside concentration-time integral ratios over a given exposure time, were calculated from the analog mass concentration records obtained from the optical sensors. The size-dependent sensor responses were corrected by weighting with the log normal parameters of the challenge and penetrating particles' spectra. The inside dose calculation is not fully accurate since the size composition of the mass concentrations is time-dependent, the particles settling out in accordance with their size distributions. With the integral

Table 1
Measured and modeled particulate protection factors

Challenge powder	Measured particle protection factor	Modeled particle protection factor	Modeled vapor protection factor
Talc	60	50	4
Sipernat D11	16	13	8
Titanium dioxide	6	6	4
Arizona road dust	5	10	6

sensor response being time-dependent, calculations based on the mass concentrations are considered first-order approximations.

Table 1 gives measured and modeled protection factor results for several candidate powder challenges under the conditions described previously. The high protection factor measured for talc is a result of the combination of considerable filtering in the slit as well as rapid gravitational settling in the chamber. It is notable that the protection factor for the relatively small titanium dioxide particles is nearly the same as for vapors since almost no filtering in the slit and minimum settling in the chamber occur.

An additional series of tests, using exposure to talc, was designed to emphasize variation of the protection factor as a function of the differential pressure across the slit. Runs were performed at pressure differentials of -10, -20 and -30 Pa across the same slit. Results of the measurements and calculations are shown in Table 2.

The experimental total transport fraction for a given pressure differential, that portion of the particles entering the slit which passed through into the enclosure, was determined by the ratio of the particle size spectrum of the initial penetrating fraction to that of the challenge cloud. To compare these results to calculations, the model output for the total transport fraction in the range 1–7 μm at a pressure differential of -10 Pa (shown in Fig. 9) was first found to closely fit a quadratic function ($r^2 = 0.995$). Fig. 10 shows experimental results and their fit to a quadratic function for the same pressure differential. The quadratic fit ($r^2 = 0.7$) and the sharp cutoff near 6.5 μm correlated well with model calculations.

4.4. Parameter sensitivity

Given that a reasonable correlation between the expected and the measured results can be obtained, the model is useful for parameter sensitivity testing. Such testing helps, for example, to determine when a significant difference between vapor and solid particle protection factors would warrant integrity testing with a solid particulate simulant, or to what extent turbulent intensity influences the removal of respirable particles. Sample model runs addressing these questions are summarized in Fig. 11. Experimental settling rates for talc are used here while all other parameter values are as previously given. Only the aperture height is changed between graphs.

Table 2
Protection factors as a function of differential pressure

Pressure (Pa)	Measured particle protection factor	Modeled particle protection factor	Modeled vapor protection factor
−10	27	18	5.5
−20	15	15	4.7
−30	10	12	3.6

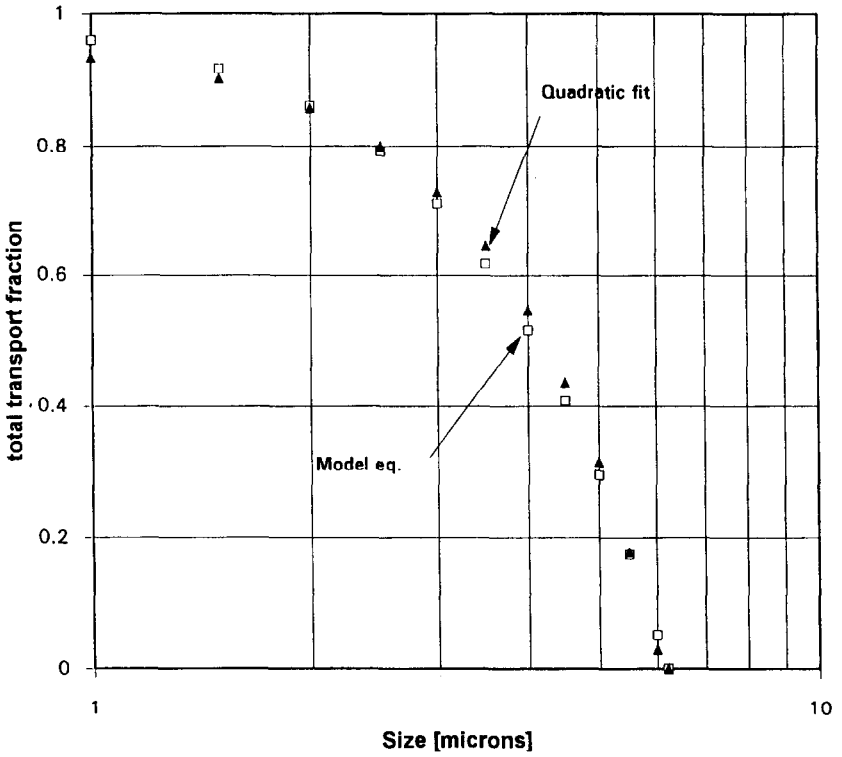

Fig. 9. Modeled total transport fraction for −10 Pa differential pressure fit to a quadratic function in the range 1–7 μm ($r^2 = 0.995$).

In each figure three sets of protection factors are plotted against the differential pressure: vapor, solid particle with quiescent (no mechanical) mixing and solid particle with turbulent (two muffin fans) mixing conditions. The figure for a 0.1 mm aperture width with turbulent mixing (Fig. 11(a)) shows the accentuated solid particle protection obtained since talc particles are both filtered out during penetration and settle out to the surfaces rapidly. The influence of turbulent impaction alone is emphasized

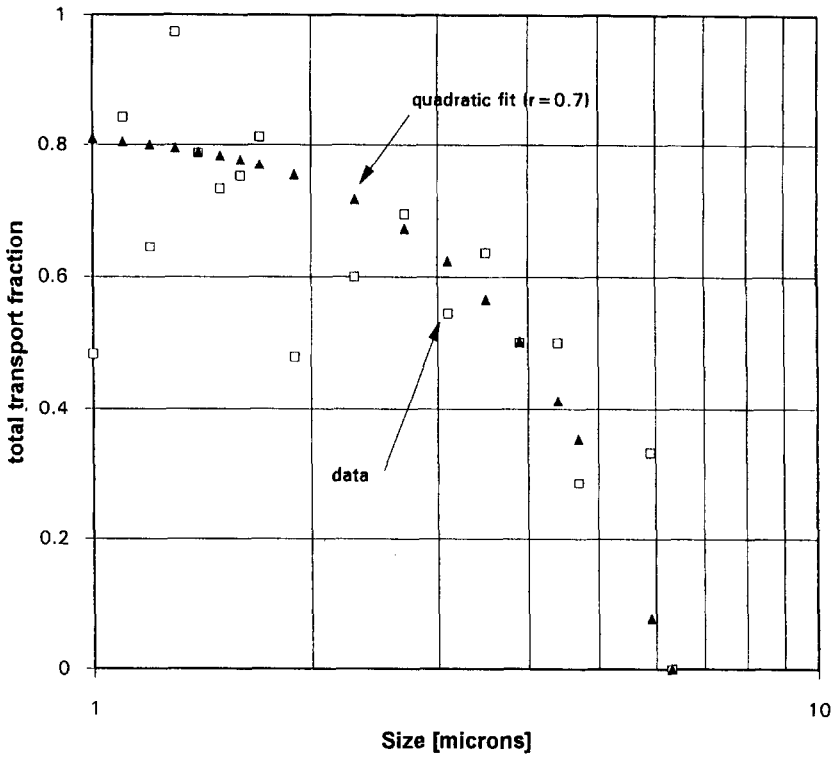

Fig. 10. Experimental total transport fraction for talc particles fit to a quadratic function in the range 1–7 μm ($r^2 = 0.7$).

by comparison to the curve for quiescent mixing where the solid particle protection factors approach those of the vapor. Here the settling rates have slowed dramatically and the particles are flushed out nearly at the same rate as vapor molecules.

With a 0.5 mm slit width (Fig. 11(b)) particle filtering is already drastically reduced and the solid particle protection factors are rapidly approaching those of the vapor, being maintained higher only for the case of turbulent mixing. The runs for 1.0 mm width (Fig. 11(c)) confirm that by this point there is practically no filtering and only the turbulent impaction provides some improvement in the particulate protection factors.

5. Conclusions

A model program has been constructed which calculates theoretical vapor and size-dependent solid particle protection factors for an enclosure with pressure-driven penetration through a well-defined aperture. The model integrates particle

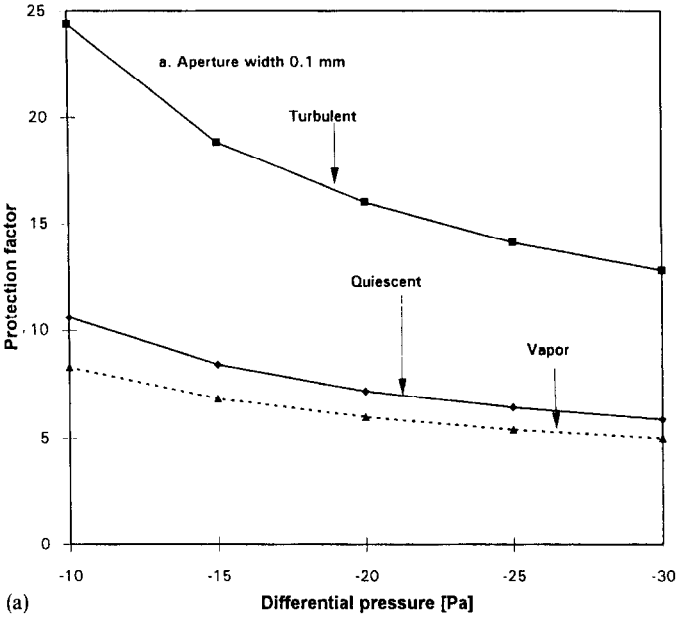

(a)

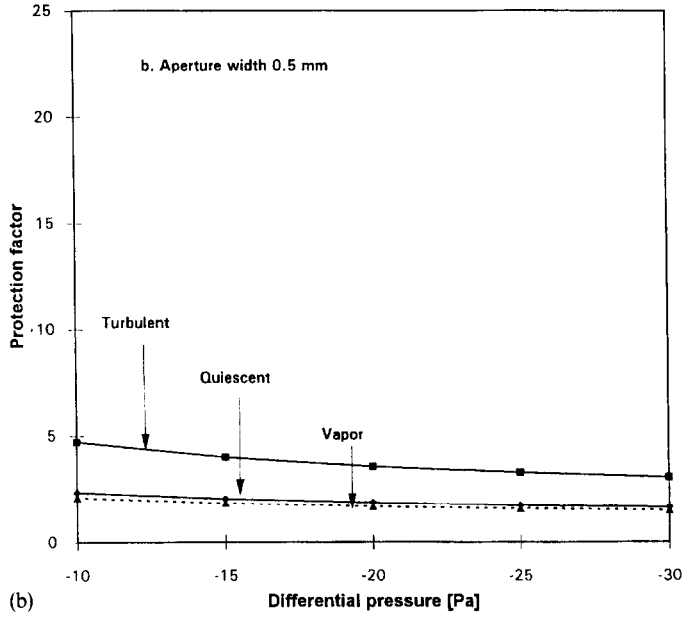

(b)

Fig. 11. Particulate and vapor protection factor model sensitivity to aperture width and mixing regime as a function of differential pressure: (a) Aperture width 0.1 mm; (b) Aperture width 0.5 mm; and (c) Aperture width 1.0 mm.

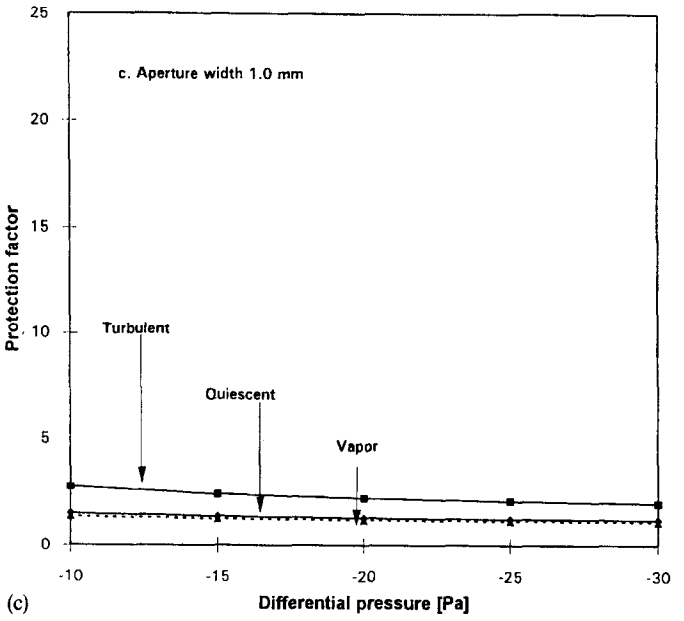

Fig. 11c.

penetration and settling rate submodels into an interactive tool designed for parameter sensitivity studies, integrity test procedure design and protection estimation.

An experimental system has been assembled which provides data on the parameters relevant to the calculation of solid particle protection factors for enclosures. The system provides empirical data for model calibration, verification and prediction. Together with the model program, the facility aids in optimizing integrity testing options for shelters and vehicles.

When combined with empirical data, model results to date correlate well with observed behavior and provide first-order protection estimates for the given enclosure. However, further work is warranted to improve characterization of particle settling in the stirred enclosure in terms of the turbulent energy content and to deal with additional phenomena such as electrostatic charges, surface effects, humidity and filtering through rough cracks.

Appendix: Protection factors for vapor and solid particles

This appendix provides a derivation of Eqs. (1) and (2) in the text which define the protection factors for vapor and solid particle penetration into enclosures. Background material for the derivations may be found in the referenced articles [3, 4]. The

primary addition here is that the exposure resulting from continued occupation of the enclosure after the challenge has passed is taken into account.

The derivation assumes spatially uniform exposure of all leakage areas to the outside challenge and that the infiltrating air carries with it the true outside concentration of challenge material at the enclosure boundary.

The enclosure is characterized by an infiltration rate, R, air changes/hour, determined by the ventilation dynamics (wind speed and stability, thermal gradients, leakage areas, etc.). Assume the enclosure to be exposed to a 'square' cloud of contaminant in which the concentration, $\mathrm{CE}(t)$, increases abruptly to a value $\mathrm{CO}(t)$ and then decreases abruptly to zero after finite time T. The rate of change of the inside concentration will be:

$$\frac{\mathrm{d}}{\mathrm{d}t}\mathrm{CI}(t) = R \cdot (\mathrm{CE}(t) - \mathrm{CI}(t)). \tag{A.1}$$

This has the solution, for $0 < t < T$ when $\mathrm{CE}(t) = \mathrm{CO}(t)$:

$$\mathrm{CI}_1(t) = \mathrm{CO} \cdot (1 - \exp(-R \cdot T)) \tag{A.2}$$

and, for $t > T$ when $\mathrm{CE} = 0$:

$$\mathrm{CI}_2(t) = \mathrm{CI}(T)\exp(-R \cdot (t - T)). \tag{A.3}$$

Hence,

$$\mathrm{CI}_2(t) = \mathrm{CO} \cdot (\exp(R \cdot T) - 1)\exp(-R \cdot t). \tag{A.4}$$

In order to calculate the dosages outside and inside the enclosure, the concentration-time integrals are required. At time $t = T$ the outside dose is

$$\mathrm{DO} = \mathrm{CO} \cdot T. \tag{A.5}$$

Inside the enclosure, for $0 < t < T$:

$$\mathrm{DI}_1 = \int_0^T \mathrm{CI}_1(t)\,\mathrm{d}t \tag{A.6}$$

and

$$\mathrm{DI}_1 = \frac{\mathrm{CO}}{R} \cdot (R \cdot T - (1 - \exp(-R \cdot T))). \tag{A.7}$$

For $t > T$:

$$\mathrm{DI}_2 = \int_T^t \mathrm{CI}_2(t)\,\mathrm{d}t. \tag{A.8}$$

Hence,

$$\mathrm{DI}_2 = \frac{\mathrm{CO}}{R} \cdot (1 - \exp(R \cdot T)) \cdot (\exp(-R \cdot t) - \exp(-R \cdot T)). \tag{A.9}$$

The protection factor is defined as the ratio of the dose which would result from exposure to the outside concentration to the dose accumulating within the enclosure up to time $t > T$:

$$\mathrm{PF} \equiv \frac{\mathrm{DO}}{\mathrm{DI}_1 + \mathrm{DI}_2}. \tag{A.10}$$

Hence,

$$\mathrm{PF}_v = \frac{R \cdot T}{R \cdot T - (1 - \exp(-R \cdot T)) + (1 - \exp(R \cdot T)) \cdot (\exp(-R \cdot t) - \exp(-R \cdot T))} \tag{A.11}$$

Reducing this yields Eq. (1):

$$\mathrm{PF}_v = \frac{R \cdot T}{R \cdot T + \exp(-R \cdot t) \cdot (1 - \exp(-R \cdot T))}. \tag{A.12}$$

Note the special case in which the cloud passage time exactly equals the inside exposure time, i.e., the occupants exit the enclosure immediately:

$$\mathrm{PF}_v = \frac{R \cdot T}{R \cdot T - (1 - \exp(-R \cdot T))}. \tag{A.13}$$

Addressing a solid particle challenge, two effects that influence the interior dosage, and, hence, the derivation of the protection factor, are the filtering of particles as they pass through the leakage areas and the deposition of particles on interior surface areas. Resuspension of particles can also affect the overall balance at a later time as can evaporation of condensed vapors, but these are not considered here. Returning to the balance equation for the enclosure, but with the filtering factor, f_p, which reduces the penetrating particle concentration, and the decay rate, β_p, which contributes to the removal of particles, we obtain

$$\frac{\mathrm{d}}{\mathrm{d}t}\mathrm{CI}_p(t) = f_p \cdot R \cdot (\mathrm{CO}_p(t) - \mathrm{CI}_p(t)) - \beta_p \cdot \mathrm{CI}_p(t). \tag{A.14}$$

The two particle removal terms can be combined into one effective term (see also Engelmann [3]:

$$R_p = R + \beta_p. \tag{A.15}$$

Hence,

$$\frac{\mathrm{d}}{\mathrm{d}t}\mathrm{CI}_p(t) = f_p \cdot R \cdot \mathrm{CO}_p(t) - R_p \cdot \mathrm{CI}_p(t). \tag{A.16}$$

Solving the equation of the form

$$\frac{\mathrm{d}X}{a + b \cdot X} = \mathrm{d}t, \tag{A.17}$$

yields

$$CI_p(t) = \frac{f_p \cdot R}{R_p} \cdot CO_p(t) - \frac{\text{const.}}{R_p} \cdot \exp(-R_p \cdot t), \tag{A.18}$$

with the given boundary conditions for $0 < t < T$:

$$CI_{p1}(t) = \frac{f_p \cdot R}{R_p} \cdot CO_p \cdot (1 - \exp(-R_p \cdot T)). \tag{A.19}$$

Solving for $t > T$:

$$CI_{p2}(t) = \frac{f_p \cdot R}{R_p} \cdot CO_p \cdot (1 - \exp(-R_p \cdot T)) \cdot \exp(-R_p \cdot (t - T)). \tag{A.20}$$

Again, doses are required for the two time periods:

$$DI_{p1} = \int_0^T CI_{p1}(t)\,dt \quad \text{and} \quad DI_{p2} = \int_T^t CI_{p2}(t)\,dt, \tag{A.21}$$

$$DI_{p1} = \frac{f_p \cdot R}{R_p} \cdot CO_p \cdot \left(T - \frac{1}{R_p} + \frac{\exp(-R_p \cdot T)}{R_p} \right), \tag{A.22}$$

$$DI_{p2} = \frac{f_p \cdot R}{R_p} \cdot CO_p \cdot (1 - \exp(R_p \cdot T)) \cdot \frac{1}{R_p} \cdot (\exp(-R_p \cdot t) - \exp(-R_p \cdot T)). \tag{A.23}$$

By definition we have

$$PF_p = \frac{DO_p}{DI_{p1} + DI_{p2}}, \quad \text{where} \quad DO_p = CO_p \cdot T. \tag{A.24}$$

Combining and reducing terms yields Eq. (2):

$$PF_p = \frac{R_p \cdot T}{\frac{f_p \cdot R}{R_p} (R_p \cdot T + \exp(-R_p \cdot t) \cdot (1 - \exp(R_p \cdot T)))}. \tag{A.25}$$

Acknowledgements

This work was performed while the author was an Exchange Scientist in the Research Directorate of the US Army Edgewood Research and Engineering Center, Aberdeen Proving Grounds, Maryland, USA. He would like to express his appreciation to the staff of the Center for their support during this period, to Dr. Arthur Stuempfle, Debbie Buckless and particularly to the members of the Ventilation Kinetics Group, Alan Seitzinger and Eric Knoebel, all of whom generously contributed of their time in making the year so fruitful.

References

[1] J. Roed, in: F. Luykx and J. Sinnaeve (Eds.), Proc. Workshop for Assessing the Off-site Radiological Consequences of Nuclear Accidents, 15–19 April 1985, EUR 10397, Luxembourg, CEC, 1986, pp. 559-599.
[2] H.D. Brenk and H. De Witt, Rad. Prot. Dosimetry, 21(1/3) (1987) 117–123.
[3] R.J. Engelmann, Atmos. Environ., 26A(11) (1992) 2037–2044.
[4] R.J. Engelmann, W.R. Pendergrass, J.R. White and M.E. Hall, Atmos. Environ., 26A(17) (1992) 3119–3125.
[5] J.F. Van de Vate, J. Colloid Interface Sci., 41(2) (1972) 194–197.
[6] A.W. Harrison, J. Colloid Interface Sci., 69(3) (1979) 563–570.
[7] J.G. Crump and J.H. Seinfeld, J. Aerosol Sci., 12(5) (1981) 405–415.
[8] J.G. Crump, R.C. Flanagan and J.H. Seinfeld, Aerosol Sci. Technol., 2, (1983) 303–309.
[9] K. Okuyama, Y. Kousaka, S. Yamamato and T. Hosokawa, J. Colloid Interface Sci., 110(1) (1986) 214–223.
[10] W. Behnke, W. Hollander, W. Koch, F. Nolting and C. Zetzsch, Atmos. Environ., 22(6) (1988) 1113–1120.
[11] R. Van Dingenen, F. Raes and H. Vanmarcke, J. Aerosol Sci., 20(1) (1989) 113–122.
[12] B.T. Chen, H.C. Yeh and Y.S. Cheng, Aerosol Sci. Technol., 17 (1992) 9–24.
[13] L.C. Schwendiman and S.L. Sutter, Transport of particles through gas leaks – a review, BNWL-2218, 1977.
[14] D. Sinclair, R.J. Countess, B.Y.H. Liu and D.H.H. Pui, Air Poll. Control Assoc. J., 26(7) (1976) 661–663.
[15] F. Kreith and R. Eisenstadt, ASME Trans., 79 (1957) 1070–1078.